PCCP

Accepted Manuscript

ROYAL SOCIETY OF CHEMISTRY

www.rsc.org/pccp

Journal Name

ARTICLE

Fabrication of transparent SERS platform via interface self-assembly of gold nanorods and gel trapping technique for on-site real time detection

Received 00th January 20xx,
Accepted 00th January 20xx

DOI: 10.1039/x0xx00000x

www.rsc.org/

Xiang Lin,[a] Wu-Li-Ji Hasi,*[a] Si-Qin-Gao-Wa Han,[b] Xiu-Tao Lou, [a] Dian-Yang Lin,*[a] Zhi-Wei Lu*[a]

A transparent SERS platform was fabricated via gel-trapping method coupled with liquid/liquid interface self-assembly technique. We employ gold nanorods as the building blocks for interface self-assembly because of their strong localized surface plasmons upon excitation by infrared radiation. Based on a "Top cover" configuration, this transparent SERS platform endows high signal reproducibility for direct detecting liquid samples by confining sample droplet into a regular shape. The Au NR PDMS platform was able to directly detect crystal violet aqueous solution down to 10 ppb level with high enhancement factor (0.87×10^5) and signal uniformity (RSD = 3.9%). Furthermore, SERS-based anti-fungal agent detection on fish scale was demonstrated by simply covering the fish scale with a tailored GNRs PDMS film. The experimental results clearly show that the Au NR PDMS SERS platform has great potential for on-site real time detection of contaminant in water as well as on curving surfaces.

Introduction

Surface-enhanced Raman scattering (SERS) is a nondestructive analytical technique with unique spectroscopic fingerprints, ultrahigh sensitivity, the possibility of multiplex analysis, and simple sample preparation requirements.[1–3] Hence, SERS has several advantages compared to traditional chromatography-based methods especially in rapid detection on the spot.[4–7] With rapid developments and advances of advanced Raman spectrometer and high performance SERS substrates in recent years, ultrahigh sensitivity has been demonstrated using various SERS substrates.[8–10] Single molecule level sensitivity has been observed in silver colloid system using R6G as probe molecular as early as 1997,[11] and femto[12] even atto[13] mole sensitivity also has been obtained on solid SERS substrates. Therefore, the sensitivity is no longer a problem for the application of SERS detection. However, aiming at on-site instant quantitative SERS detection, there still some problems to be resolved. For example, highly ordered SERS substrate is crucial for giving a reproducible SERS signal. In addition, uniform distribution of target sample on SERS substrate is also important.

In recent years, self-assembly technique such as droplet evaporation,[14-16] Langmuir-Blodgett[17-19] and liquid-liquid interfacial self-assembly[20-24] have been widely used to construct wafer scale periodic nanostructures from individual metal nanoparticle building blocks. The size and shape of individual metal nanoparticle can be readily controlled via wet-chemical synthesis.[25, 26] Given to the convenience and versatility, the interest in using this technique to fabricate highly uniform SERS substrates has been grown. Among the three strategies, liquid-liquid interfacial self-assembly is the most simple, robust and cost-effective method. What's more, the metal-like liquid films of nanoparticle formed at the liquid–liquid interface could access analytes from either of the phases, which gives the metal-like liquid films an unique ability to detect both water-soluble and insoluble analytes.[20, 22] Currently, the building blocks for liquid–liquid interface assembly are almost limited to gold/silver spherical nanoparticles, which in general leads to weak SERS signals. Very few reports are available on the liquid-liquid interface self-assembly of gold nanorods which is one of the most efficient structures for SERS applications.[27-31] The challenges associated with the interfacial assembly of gold nanorod are mainly related to the destabilization and partial aggregation during surfactant exchange.[19, 32] Cheng et al. used sequential "grafting to" (ligand exchange) and "grafting from" (surface initiated atom transfer radical polymerization) reactions to synthesize amphiphilic gold nanorod with mixed polymer brushes which can spontaneously assemble into two-dimensional arrays at oil/water interfaces.[21] However, the entire surface modification process is complicated and time consuming. The modified ligands used are difficult to achieve and may cause interference for SERS detection.

Despite the high uniformity of SERS substrate, the evenness of the sample distribution is another critical factor for uniform

[a] National Key Laboratory of Science and Technology on Tunable Laser, Harbin Institute of Technology, Harbin, 150080, China. E-mail: hasiwuliji@126.com; dianyanglin@hit.edu.cn; zw_lu@sohu.com.
[b] Affiliated Hospital of Inner Mongolia University for the Nationalities, Tongliao, 028007, Inner Mongolia, China.

Electronic Supplementary Information (ESI) available: [details of any supplementary information available should be included here]. See DOI: 10.1039/x0xx00000x

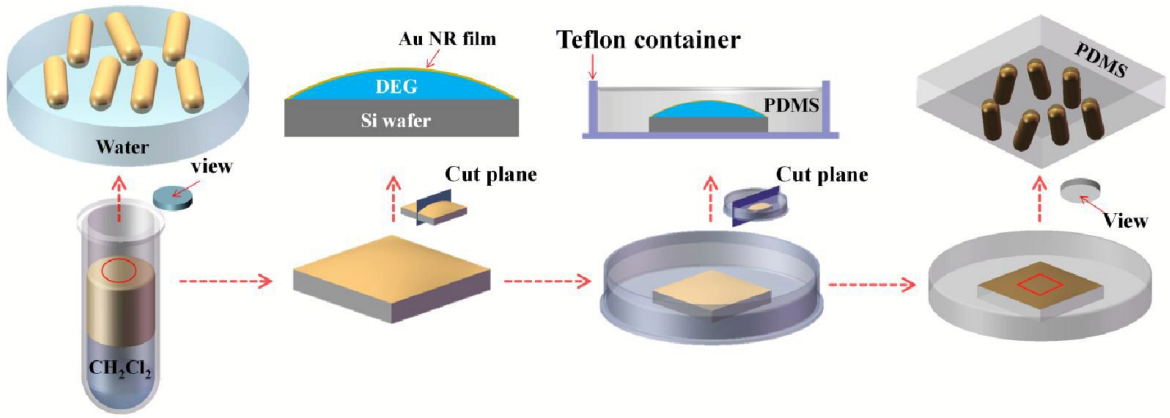

Fig. 1 Schematic illustration of Preparation of GNR PDMS substrate

SERS response. Most of SERS measurements using solid SERS substrates were operated in dried condition to obtain a higher sensitivity.[33–35] While the dried sample droplets always have an uneven distribution and the drying process is time-consuming. For the wet condition (loading a sample droplet freely on the substrate), the sample droplet forms a hemisphere morphology on hydrophobic substrate or spread randomly on hydrophilic substrate.[18, 36] The hemisphere morphology on hydrophobic substrate would cause different reflection extinction at different position and the random distributed sample was easy boil away under laser irradiation. Poor uniformity of SERS response was achieved in both situations. Recently, due to the high elasticity, high swelling and adsorption capability and excellent optical transparency of polydimethylsiloxane (PDMS), several novel metal nanoparticle–PDMS nanocomposites have been developed for various application.[37–39] Singh et al took advantage of the high elasticity of PDMS to fabricate a buckled PDMS silver nanorod arrays as active 3D SERS cages for traping and enhancing the Raman signal of P. aeruginosa bacteria.[40] Based on the high swelling and adsorption capability of PDMS, Yao et al coated a PDMS film on Au nanoparticle monolayer to fabricate a novel metal-organic frameworks (MOFs) SERS platform for improving SERS detection of aromatic molecules in water and in the atmosphere.[41] By contrast, based on the excellent optical transparency of PDMS, LizMarz´an et al coated Au nanostars on cured PDMS film to fabricate a transparent SERS platform for detecting pesticide on fruit skin.[37] In this way, PDMS plays a role as scaffold rather than host for trapping target molecular. The thickness, shape or size of PDMS can be easily tuned and SERS signals can be measured through backside irradiation and SERS collection.[37, 38] We hypothesize that transparent SERS substrates with flat morphology are able to address the aforementioned limitations of solid SERS substrates by confining sample droplets into a regular shape. Thereby the real-time quantitative determination can be achieved.

In this paper, citrate-stabilized gold nanorods have been prepared by surfactant exchange from CTAB-coated GNRs, which possess a cleaner and active plasmonic surface. A facile and robust method was developed to assemble citrate stabilized gold nanorods on liquid/liquid interface. No other modifier agents were employed to promote assembly of NRs at the interface in this protocol. The density of gold nanorods on the interface can be tuned by changing the concentration of gold nanorods solution or the angle of the container. Gel trapping technique was employed to transfer Gold nanorods onto PDMS scaffold to fabricate the transparent SERS platform with a square hole inside a circle. The SERS signal reproducibility of the PDMS GNRs film under two different configurations was characterized. The GNR PDMS platform enables quantitative and immediate detection of crystal violet down to 10 ppb in water body. The potential of the PDMS substrate for real-life applications has also been demonstrated through an example showing SERS detection of CV on fish scale. The excellent convenience and reliability of this substrate make it suitable for on-site quantitative detection of contaminants in water body as well as on non-flat surfaces, potentially serving as a versatile platform for environment monitoring and fast food screening.

Experimental

Chemicals

Hexadecyltrimethylammonium bromide (CTAB H6269) and sodium polystyrenesulfonate (Na-PSS, Mw= 70 kDa) were purchased from Sigma Aldrich. Sodium oleate (NaOL, > 97.0%) was purchased from TCI Shanghai. Chloroauric acid hydrate ($HAuCl_4{\cdot}4H_2O$), Silver nitrate ($AgNO_3$) and sodium citrate were obtained from Sinopharm Chemical Reagent Co., Ltd., PDMS was obtained from Dow Corning, USA (Sylgard 184); Crystal violet (CV) was obtained from Tianjin Guangfu Fine Chemical Research Institute co., Ltd., All solutions and dilutions were prepared using ultrapure water with a resistivity larger than 18.2 MΩcm.

Preparation of Citrate-Stabilized GNRs

Original Gold nanorod suspensions were prepared by using the binary surfactant mixture (CTAB + NaOL) reported by Murray's group.[42] The as prepared CTAB-GNRs were converted into

Citrate-Stabilized-GNRs (Cit-GNRs) according to Wei's method.[32] Briefly, the GNRs solution (optical density (O.D.) = 2.4) were subjected to three cycles of centrifugation and redispersion in 0.05 wt % Na-PSS (Mw= 70 kDa) to deplete CTAB to trace levels. The PSS-GNRs were then subjected to two additional C/R cycles using 2 mM sodium citrate for exchange with PSS, yielding stable dispersions of citrate coated GNRs (O.D. = 1.19).

Interfacial self-assembly of GNRs

The Liquid-liquid interfacial self-assembly of GNRs was performed using a previously described method with slight simplification.[20] Firstly, 1 mL of Cit-GNRs and 1 mL CH_2Cl_2 were added into a 5 mL centrifuge tube (Teflon) and the mixture was vigorous shaken for 1 min. After standing for a 30 s, a brilliant golden film was formed spontaneously on the interface of water and dichloromethane (CH_2Cl_2). Due to the Teflon wall is oleophilic and highly hydrophobic, the GNRs interfacial film was wrapped around the upper water layer and part of the GNRs interfacial film was exposed to the air (Fig. 1, Fig. S1).

Fabrication of GNR PDMS substrate

Gel-trapping method was used to transfer Au NR interface film onto the PDMS mold (Fig. 1, Fig. S1).[39,43] Silicon wafer (5mm × 5mm) was pretreated to render its surface hydrophilic by washing it with acetone and then filling in an $NH_3 \cdot H_2O$ (28%)/H_2O_2 (30%) (1/1 v/v) mixed solution at 100°C, followed by washing with enough water and drying in air. Then, silicon wafer was immersed into diethylene glycol (DEG) followed by putting on a filter paper. Afterwards, silicon wafer was dipped into the GNRs interfacial film and then horizontal lifted up. Therefore, the GNRs interfacial film was transferred onto the DEG/water interface supported by silicon wafer. Silicon wafer was then placed into the bottom of Teflon wall (inner diameter, 1 cm), after which 250 μL of premixed PDMS precursor mixture (10:1; elastomer: curing agent) was poured into the Teflon wall and the container was left at 60℃ for the PDMS to cure. After the PDMS was hardened (3 hours), it was lifted off from the container and silicon wafer. Finally, the GNRs loaded PDMS film was washed in warm water to remove residual DEG.

Characterization

Transmission electron microscopy (TEM) was performed with a Tecnai G2 20 TWIN Transmission Electron Microscope. Scanning electron microscopy (SEM) images were collected using a Hitachi SU8010 field emission scanning electron microscope at an accelerating voltage of 15 kV. Because of the insulativity of PDMS, a very thin (~10nm) Pt film was sprayed onto the GNRs PDMS substrate to obtain a SEM picture as clearly as possible. UV-vis absorption spectra were recorded on a Cary 4000 UV-vis spectrophotometer with a quartz cuvette of 1 cm optical path length.

SERS Measurements

Normal Raman and SERS spectra were acquired using a portable compact laser Raman Spectrometer (BWS415-785H, B&W Tek). Since the surface plasma resonance (SPR) absorption peak of Au NRs PDMS film lies in the near-infrared region and longer laser excitation wavelengths do not have enough energy to excite molecular fluorescence, a 785 nm laser has been used as the excitation light to avoid fluorescence interference. The spectrometer provides Raman spectrum over the range of 175 to 2700cm^{-1} with a spectral resolution of better than 3 cm^{-1}. The laser power ranges from 30 to 60 mW in this study. The typical exposure time for protein measurements was 5 s unless otherwise stated. In the normal Raman and SERS experiments, the laser beam was directly focused on the substrates and spectra were collected upon backside laser irradiation. In the SERS experiments, 15 μL of sample solution was dropped onto hydrophobic aluminum tape which is stuck on a glass slide. Then the Au NR PDMS platform was coated onto the sample droplet. Finally, the platform was illuminated from the backside with a 785 nm laser. All the spectra were present after smooth and baseline correction.

Results and discussion

As determined by TEM (Fig. 2A), the length and diameter of the prepared GNRs are 90 ± 3 nm and 30 ± 1.2 nm, respectively, leading to an aspect ratio of 3. The UV-vis-NIR spectrum of GNRs colloid showed two absorption bands at 512 nm and 730 nm corresponding to the transverse surface plasma resonance (TSPR) and the longitudinal surface plasma resonance (LSPR), respectively (Fig. 2C). The relative narrow width of the LSPR indicated the monodispersity of the prepared GNRs. The as prepared CTAB stabilized GNRs were converted into Citrate Stabilized GNRs (Cit-GNRs) according to Wei's method via intermediate treatment with PSS. The LSPR position of citrate-stabilized GNRs has a very slight blue-shift (~3 nm) compared with CTAB GNRs, indicating the effective exchange of the capping ligand. The color of citrate-stabilized GNRs solution (the second photograph in Fig. 2C) and the shape of absorption spectrum indicate that no nanorod aggregation occurred. The citrate-stabilized GNRs have similar surface properties as other citrate-stabilized nanoparticles. Consequently, the liquid-liquid interfacial self-assembly method which has been widely applied for metal nanoparticles is applicable to citrate stabilized GNRs. Better yet, a metal-like liquid film of GNRs could form on the liquid-liquid interface without using any promoter. Once GNRs assembled on the interface, the color of GNRs colloid was changed from dark orange to deep brown (the third photograph in Fig. 2C). The metal-like liquid film exhibit excellent mechanical robustness, and it could keep a uniform distribution even subject multiple shaking (Fig. S3). The density of GNRs could be adjusted by verifying the angle of the container or the concentration of GNRs colloid (Fig. S4). Overall, this strategy is more convenient, robust, controllable and flexible than other self-assembly technologies such as Langmuir-Blodgett methodology. Moreover, GNRs coated with citrate are more suitable for first layer reactions such as SERS due to the weak binding activity of citrate anion.[44]

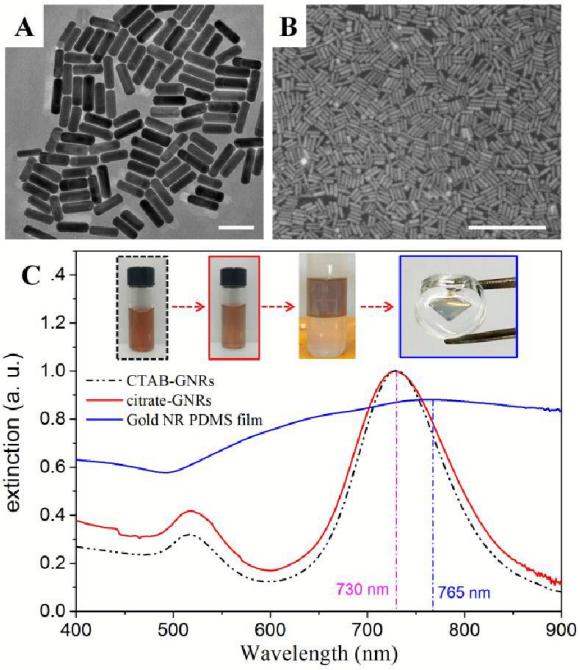

Fig. 2 (A) SEM images of Au NRs deposited on silicon film. Scale bar, 100 nm. (B) Au NR PDMS substrate coated with a 10 nm Pt film. Scale bar, 500 nm (C) UV/vis/NIR absorbance spectra of the Au NRs colloid solution before (black) and after (red) capping agent exchange and the Au NR PDMS substrate. Insets: photographs of the Au NRs colloid solutions, liquid-liquid interface film and Au NR PDMS substrate.

Afterwards, the metal-like liquid Au NR film was transferred onto PDMS mold via gel-trapping method (Fig. 1, Fig. S1). The PDMS platform was casted to the structure with a square hole inside a circle. The inner area is plain and the height of the inner cavity is about 0.5 mm. This flat cavity could confine the hemispheric droplet into a regular shape with uniform height. The PDMS substrates were characterized by UV-vis spectroscopy and SEM (blue line in Fig. 2C and Fig. 2B). SEM image of the Au NRs PDMS film shows that a uniform Au NR monolayer was coated on PDMS substrate. No Au NR aggregates were generated and only few nanocubes were observed. The extinction spectra of the prepared substrates revealing a broad LSPR peak at 765 nm for the GNRs PDMS film. The broadening and shift of the extinction maximum on the spectrum of GNRs PDMS film with respect to their colloidal suspension were due to the strong plasmonic coupling effect of the unordered and close arranged Au NRs monolayer.[45] Moreover, since the monolayer of Au NR can be scraped off from the PDMS substrate by a knife, Au NRs were actually covered on the PDMS film rather than embed in it.

In most cases, the SERS sensitivity of SERS substrates fabricated via interface self-assembly technique is strongly dependent on the density of building blocks.[7, 46, 47] To optimize the SERS sensitivity of Au NR PDMS platform, different concentration of GNRs were assembled on PDMS film. The photographs of metal-like liquid films with different nanorod concentrations before transferred to PDMS film were shown in Fig. S4. By changing the concentration of initial GNR solution, the color of the GNR monolayer at the water-oil interface changes from yellow red (O.D. = 1.19) to deep brown (O.D. = 4.76) with golden reflection, as observed from the digital photo of Fig. S4D. The changes in reflection color is because of the changes in plasmonic coupling between adjacent nanorods during the assembly. The coverages of the Au NRs deposited on silicon wafer with different concentrations were characterized by SEM (Fig. 3A-D). The SEM images indicated an increased coverage (27.9%, 44.5%, 52.3% and 69.0%) and improved uniformity of the substrate as the concentration of Au NPs increases. The photograph in Fig. 3E are Au NR PDMS platforms with different Au NR concentrations. The colors of the substrate gradually deepen as GNR coverage increased. Crystal violet (CV), which is an unapproved drug that could effective against fungal and parasite infections in fish, was employed as the probe molecule for SERS measurements.[48]

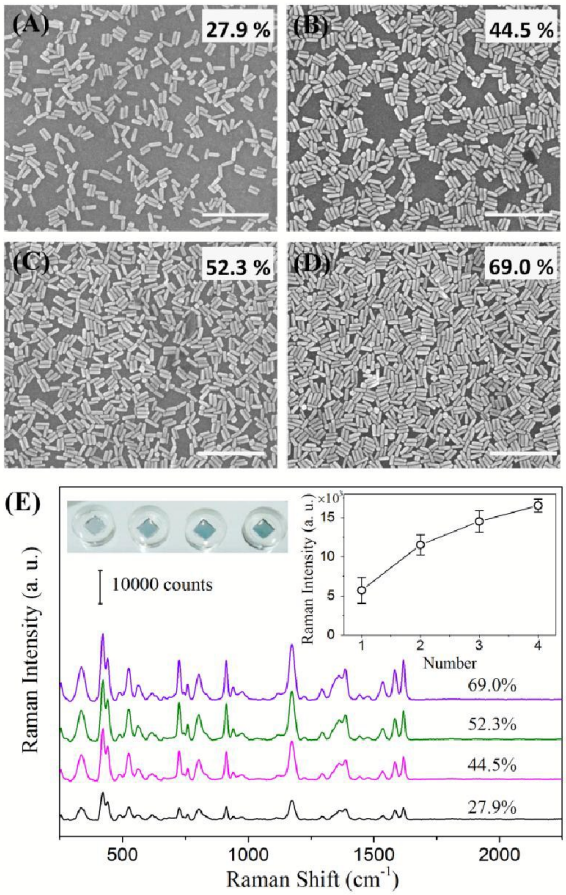

Fig. 3 (A-D) SEM images of GNR monolayer with coverages of 27.9%, 44.5%, 52.3% and 69.0%. Scale bar, 500 nm. The coverage of Au nanorod was adjusted by changing the concentration of original GNRs solution. (E) SERS spectra of 10^{-5} M CV on GNR PDMS substrate with different coverages. Insert: photograph of the prepared GNR PDMS substrate with different coverages (increasing from lift to right) and the SERS intensity of the 1174 cm^{-1} band on PDMS substrates with different Au NR coverage.

The strong bands at 416 and 722 cm^{-1} were due to out of-plane bending mode of C–C–C and C–N–C symmetric stretching vibration of dimethylamino group, respectively. The medium bands at 521 and 557 cm^{-1} were assigned to bending mode of C–N–C and out-of-plane aromatic C–C deformation. Bands at 913 and 819 cm^{-1} were attributed to the C–H out-of-plane bending modes. The strong Band at 1174 cm^{-1} was due to the

C–H in-plane bending mode. Bands at 1357 and 1389 cm^{-1} were origin from overlap of stretching vibration of C–C–C and stretching vibration of nitrogen and phenyl ring. Bands at 1582 and 1615 cm^{-1} were due to in-plane aromatic C–C stretching vibration.[49, 50] As mentioned above, Au NRs were coated on the PDMS film rather than embed in it, thus target molecules would directly interact with Au NRs. The interaction between PDMS and target molecules would not influence the SERS detection performance. Fig. 3E shows the SERS spectra of 10^{-5} M CV solution using PDMS substrates with different Au NR concentrations. SERS intensity of CV solution collected on Au NR PDMS platforms increases with Au NR concentration (as shown in the Figure insert on the right side of Fig. 3E). From here onwards, Au NR PDMS films with coverage of 69.0% (corresponding to an optical density value of 4.76 for Cit-GNR solution) are used for further analysis.

Another critical aspect for routine SERS application is to ensure a reliable and excellent signal reproducibility. Because of the optical transparency and 3D structure of PDMS substrate, two kinds of detection modes were available for this transparent substrate. SERS signals were collected and compared from either of two sides as shown in Fig. 4B and E (Top cover, 15 μL of sample solution was dropped on a hydrophobic surface such as aluminum tape, then the droplet was covered by PDMS SERS platform with nanorods on the bottom side; Bottom support, a droplet of sample solution was directly dropped onto the PDMS SERS platform with nanorods on the top side, in a same way as conventional strategy based on rigid opaque substrates). As shown in Fig. 4I, the bands position and intensity of SERS spectra collected from the center area of GNR PDMS films in the two detection ways were almost identical. However, the bands intensity of SERS spectra collected from the non-center area of GNR PDMS films in the two detection ways were very different. To systematically evaluate the uniformity of the Raman intensity acquired from a droplet sample using the two detection ways, the Raman probe was scanned through the diagonal of PDMS substrates, as shown in Fig. 4B and E. The center of GNR area were set as the original points, then SERS mapping measurements were taken along the diagonal (from -3.5 mm to 3.5 mm with a step size of 0.25 mm), which ranged from one the corner to the opposite. The SERS intensities of 10^{-5} M CV at ~1174 cm^{-1} were collected to monitor intensity change, as shown in Fig. 4J. The SERS signal showed a sudden drop at the border of the GNR area for both the two configurations due to the random reflection of light by the edge. For the Bottom support mode, the Raman intensity distribution is center symmetric and gradually decreases from the center to edge. For the Top cover mode, excluding the signal from the corner, the SERS signal acquired within the Au NR area is relatively uniform with a 3.92% deviation of the average signal along the diagonal. This is attributed to the fact that the top cover mode provides a flat morphology for the reflection of incident light, while the bottom support mode provides a droplet profile which causes different reflection and refraction between the center and non-center area.[36] The reflection and refraction condition under the two configurations were illustrated in Fig. 4C and F. Here upon, Top cover mode was used for further analysis due to the uniform SERS response. Additionally, the batch-to-batch reproducibility testing was carried out by detecting SERS spectra of CV from 15 batches of the SERS substrates (Fig. S5). The relative standard deviation of the absolute signal height at 1174 cm^{-1} on 15 different substrates is 9.1%, revealing a good batch to batch reproducibility of the Au NR PDMS platform.

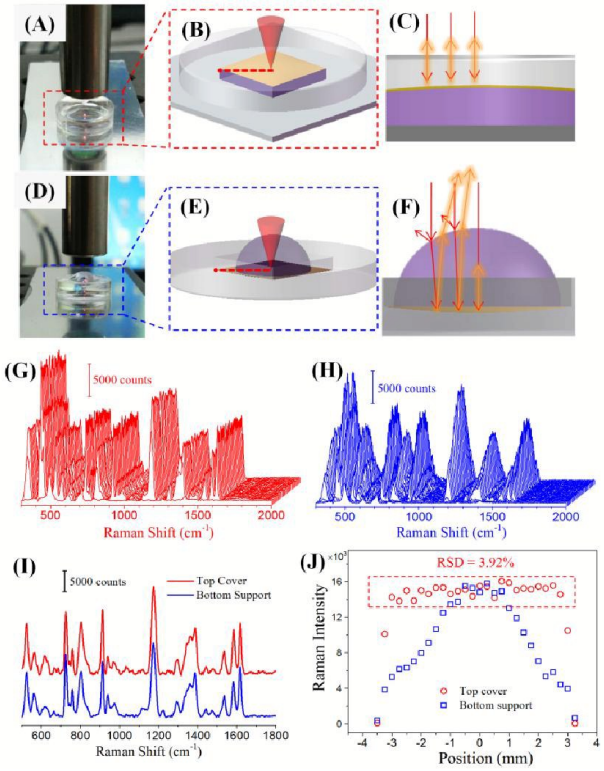

Fig. 4 The photographs and schematics of top cover (A, B, C) and bottom support (D, E, G) configurations for SERS measurement using GNR PDMS substrate. (G, H) Line SERS mapping measured on the substrate along the diagonal under the two configurations, the increment was 0.25 mm. (I) SERS spectra collected from the center area of PDMS AuNR films in the two detection ways. (J) Line SERS mapping of SERS band at 1174 cm^{-1} measured on the substrate along the diagonal of GNR PDMS substrate.

To test the sensitivity of the Au NR PDMS platform for directly detecting aqueous samples, crystal violet (CV) aqueous solutions with different concentration were subjected to SERS detection using the PDMS substrates. Fig. 5A shows the recorded SERS spectra of CV. The minimum detectable concentration of the PDMS substrate was 10 ppb for CV. The analytical enhancement factor (EF) of the GNR PDMS substrate was found to be as high as 0.87×10^5 for directly detection of liquid sample (Fig. S6). As shown in Fig. 5B, within the concentration range of 0.01 to 1 ppm, SERS intensity of CV increase linearly along with the growth of concentration. The equation of the calibration curves is $y = 1091 + 11977x$ with $R^2 = 0.985$ (Fig. 5B), where y and x represent the SERS intensity and the concentration of CV, respectively. The limit of quantification (LOQ) could be determined to be ~ 2.45×10^{-8} M. However, as the concentration of CV further increase, the grown of peak intensity is tend to saturation. This phenomenon can be attributed to the saturated adsorption of sample molecules on

metallic surface since SERS effect is a first layer effect.[44, 51] Due to the SERS measurement of liquid samples could be conducted immediately, real-time on-site quantitative analysis of CV in water body can be achieved using this PDMS SERS substrate without additional sample-processing steps.

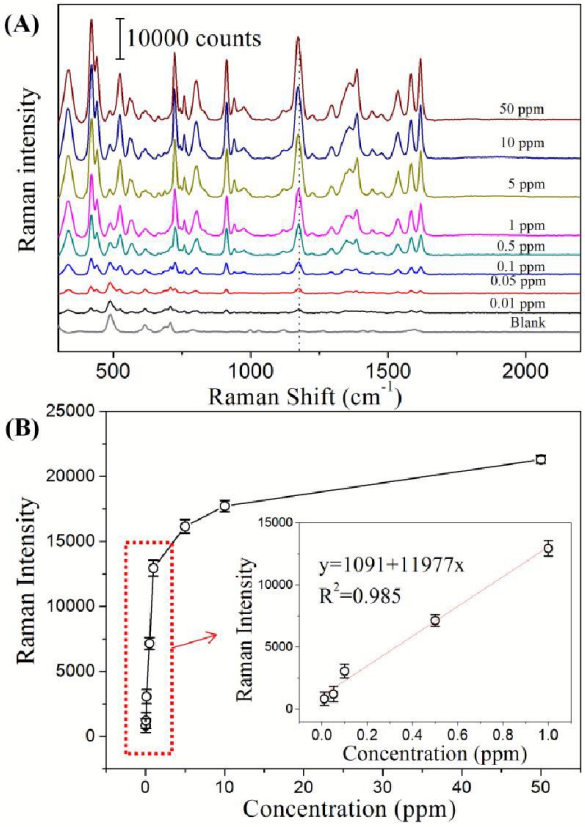

Fig. 5 (A) SERS spectra of aqueous CV at various concentrations. (B) SERS intensities at 1174 cm^{-1} for CV concentration ranging from 10 ppb to 50 ppm. Insert: Linear calibration plot at low CV concentration.

Even the LOQ for detecting CV is higher than the maximum allowable limit (0.5 ppb) according to the EU criteria, considering the fast and simple of SERS method compare with other approaches, SERS detection based on this substrate can also serve as an effective method for fast screening of fish samples. It could eliminate presumptive negative samples of CV from the sample population, and then check presumptive positive samples using other complicated laboratory equipment. Therefore, introducing the SERS method could provide a more rapid and cost-effective way for monitoring CV in large numbers of fish products.[52] On the other hand, in this paper we have developed a facile approach to assemble CTAB stabilized gold nanorods into an interfacial monolayer film. Thus the sensitivity of the PDMS platform can be improved by replacing Au nanorods with other CTAB or CTAC stabilized nanoparticles such as Ag nanocubes and Ag/Au nanorods as building blocks and using their optimal laser source.[53]

As the platform is transparent and can be cut into arbitrary shape, the gold nanorods on PDMS film have opportunity to closely contact target analyte on surface. Such substrates can thus be applied to detect chemical composition on curving surfaces, by simply coating them with Au NR PDMS films and using back side illumination. To implement this scheme, the thicker parts of PDMS surrounding the GNRs area were cut off to ensure that the GNRs could contact closely with the molecular on curving surface. Then the tailored GNR PDMS film was applied to detect CV on fish scale. Fig. 6 showed that no evident Raman signals of CV were recorded when a laser was directly light onto the fish scale with the CV molecule but without the SERS substrate, as well as from non-contaminated fish scale covered with the Au NR PDMS substrate. On the contrary, if the GNR PDMS film was coated on the fish scale contaminated with CV, significantly Raman signal of CV was detected. The Raman band of CV was clearly shown even when the concentrations were reduced to 0.1 ppm. This method is expected to extend to other applications such as detection of residual pesticides on fruit or vegetable surface.

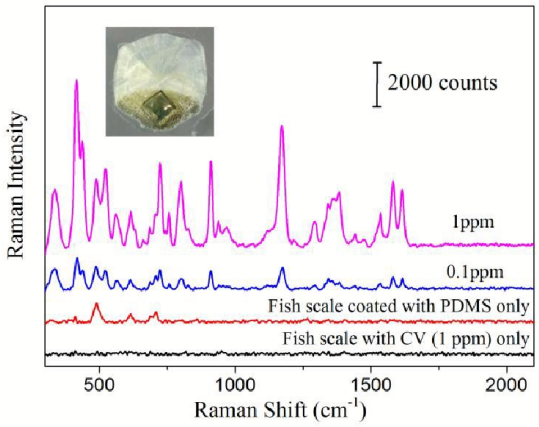

Fig. 6 SERS spectra of CV spiked on fish scale, acquired by coating the GNR PDMS film on the fish scale and then illuminating from the backside with a 785 nm laser. Control spectra were obtained from fish scale coated with a GNR PDMS film but without CV (red line) and fish scale loaded with 1 ppm CV only (black line). Insert: a schematic representation of the detection on fish scale.

Conclusions

In summary, gold nanorods were directly assembled at liquid/liquid interface without using any other "promoter" agent. The protocol is facile and robust and the density of GNRs on the interface can be readily tuned by changing the concentration of GNR solution and the angle of the container. Gel-trapping technique was employed to transfer Au NR interfacial film onto PDMS mold to fabricate the transparent SERS platform. The PDMS platform enables quantitative and immediate detection of crystal violet down to 10 ppb in water with high signal uniformity using a "Top cover" configuration. The excellent transparency of PDMS offers additional advantages for detection of contaminant on curving surfaces, which was demonstrated through the detection of CV on fish scale using back side illumination. On the basis of these unique attributes, it will open up an opportunity for the use of Au NR PDMS platform towards on-site instant SERS detection of trace containments in real world applications.

Acknowledgements

The work was supported by the International S&T Cooperation Program of China (Grant No. 2011DFA31770).

Notes and references

1 C. Haynes, A. McFarland, and R. Duyne, *Anal. Chem.*, 2005, **77**, 338A–346A.
2 D. Cialla, A. März, R. Böhme, F. Theil, K. Weber, M. Schmitt, and J. Popp, *Anal. Bioanal. Chem.*, 2012, **403**, 27–54.
3 S. Schlücker, *Angew. Chemie*, 2014, **53**, 4756–95.
4 R. S. Golightly, W. E. Doering, and M. J. Natan, *ACS Nano*, 2009, **3**, 2859–69.
5 J. Zheng and L. He, *Compr. Rev. Food Sci. Food Saf.*, 2014, **13**, 317–328.
6 K. J. Si, P. Guo, Q. Shi, and W. Cheng, *Anal. Chem.*, 2015, **87**, 5263–9.
7 L. Zhong, J. Yin, Y. Zheng, Q. Liu, X. Cheng, and F. Luo, *Anal. Chem.*, 2014, **86**, 6262−6267.
8 A. Shiohara, Y. Wang, and L. Liz-Marzán, *J. Photochem. Photobiol. C Photochem. Rev.*, 2014, **21**, 2–25.
9 T. . Jana, N. R.;Pal, *Adv. Mater.*, 2007, **19**, 1761–1765.
10 L. Polavarapu and L. M. Liz-Marzán, *Phys. Chem. Chem. Phys.*, 2013, **15**, 5288–300.
11 and S. R. E. Nie, Shuming, *Science (80-.).*, 1997, **275**, 1102–1106.
12 B. Peng, G. Li, D. Li, S. Dodson, Q. Zhang, J. Zhang, and Y. H. Lee, *ACS Nano*, 2013, **7**, 5993–6000.
13 C.-C. Yu, S.-Y. Chou, Y.-C. Tseng, S.-C. Tseng, Y.-T. Yen, and H.-L. Chen, *Nanoscale*, 2015, **7**, 1667–77.
14 S. Gómez-Graña, J. Pérez-Juste, R. a. Alvarez-Puebla, A. Guerrero-Martínez, and L. M. Liz-Marzán, *Adv. Opt. Mater.*, 2013, **1**, 477–481.
15 Z. Zhang and M. Lin, *J. Mater. Chem. C*, 2014, **2**, 4545.
16 T. Thai, Y. Zheng, S. H. Ng, S. Mudie, M. Altissimo, and U. Bach, *Angew. Chem. Int. Ed. Engl.*, 2012, **51**, 8732–5.
17 K. M. Schulz, S. Abb, R. Fernandes, M. Abb, A. G. Kanaras, and O. L. Muskens, *Langmuir*, 2012, **28**, 8874–8880.
18 H. K. Lee, Y. H. Lee, Q. Zhang, I. Y. Phang, J. Ming, R. Tan, Y. Cui, and X. Y. Ling, *ACS Appl. Mater. Interfaces*, 2013, **5**, 11409–11418.
19 Y. H. Lee, C. K. Lee, B. Tan, J. M. Rui Tan, I. Y. Phang, and X. Y. Ling, *Nanoscale*, 2013, **5**, 6404–12.
20 M. P. Konrad, A. P. Doherty, and S. E. J. Bell, *Anal. Chem.*, 2013, **85**, 6783–6789.
21 Cheng L, Liu A, Peng S, *ACS Nano*, 2010, **4**, 6098–6104.
22 M. P. Cecchini, V. a Turek, J. Paget, A. a Kornyshev, and J. B. Edel, *Nat. Mater.*, 2013, **12**, 165–71.
23 P. Guo, D. Sikdar, X. Huang, K. J. Si, B. Su, Y. Chen, W. Xiong, L. W. Yap, M. Premaratne and W. Cheng, *J. Phys. Chem. C*, 2014, **118**, 26816–26824.
24 K. J. Si, D. Sikdar, Y. Chen, F. Eftekhari, Z. Xu, Y. Tang, W. Xiong, P. Guo, S. Zhang, Y. Lu, Q. Bao, W. Zhu, M. Premaratne and W. Cheng, *ACS Nano,* 2014, **8**, 11086–11093.
25 X. Xia, J. Zeng, Q. Zhang, C. H. Moran, and Y. Xia, *J. Phys. Chem. C*, 2012, **116**, 21647–21656.
26 J. Xiao and L. Qi, *Nanoscale*, 2011, **3**, 1383.
27 W. Wei and G. Ge, *Part. Part. Syst. Charact.*, 2013, **30**, 837–841.
28 A. Mart, A. Pescaglini, C. Schopf, V. Scardaci, R. Coull, L. Byrne, and D. Iacopino, *J. Phys. Chem. C*, 2014, **118**, 13260–13267.
29 M. Tebbe, M. Maennel, A. Fery, N. Pazos-Perez, R. A. Alvarez-Puebla, *J. Phys. Chem. C*, 2014, **118**, 28095–28100.
30 H. S. Han, J. Song, J. Hong, D. Kim, and T. Kang, *Anal. Chem.*, 2014, **86**, 6160–6165.
31 R. a Alvarez-Puebla, A. Agarwal, P. Manna, B. P. Khanal, P. Aldeanueva-Potel, E. Carbó-Argibay, N. Pazos-Pérez, L. Vigderman, E. R. Zubarev, N. a Kotov, and L. M. Liz-Marzán, *Proc. Natl. Acad. Sci. U. S. A.*, 2011, **108**, 8157–61.
32 J. G. Mehtala, D. Y. Zemlyanov, J. P. Max, N. Kadasala, S. Zhao, and A. Wei, *Langmuir*, 2014, **30**, 13727–13730.
33 X. Li, H. K. Lee, I. Y. Phang, C. K. Lee, and X. Y. Ling, *Anal. Chem.*, 2014, **86**, 10437–10444.
34 J. Xu, J. Du, C. Jing, Y. Zhang, and J. Cui, *ACS Appl. Mater. Interfaces*, 2014, **6**, 6891–6897.
35 H. Wang, J. Fang, J. Xu, F. Wang, B. Sun, S. He, G. Sun, and H. Liu, *Analyst*, 2015, **140**, 2973–8.
36 X. Lin, W. Hasi, X. Lou, S. Lin, F. Yang, B. Jia, D. Lin, and Z. Lu, *RSC Adv.*, 2014, **4**, 51315–51320.
37 A. Shiohara, J. Langer, and Luis M. LizMarz´an, *Nanoscale*, 2014, **6**, 9817–9823.
38 Y. Wang, Y. Wang, H. Wang, M. Cong, W. Xu, and S. Xu, *Phys. Chem. Chem. Phys.*, 2014, **17**, 1173–1179.
39 Y. H. Lee, W. Shi, H. K. Lee, R. Jiang, I. Y. Phang, Y. Cui, L. Isa, Y. Yang, J. Wang, S. Li, and X. Y. Ling, *Nat. Commun.*, 2015, **6**, 6990.
40 S. Kumar, D. K. Lodhi, P. Goel, N. Neeti, P. Mishra and J. P. Singh, *Chem. Commun.*, 2015, **51**, 12411–12414.
41 C. Qian, Q. Guo, M. Xu, Y. Yuan and J. Yao, *RSC Adv.*, 2015, **5**, 53306–53312.
42 X. Ye, C. Zheng, J. Chen, Y. Gao, and C. B. Murray, *Nano Lett.*, 2013, **13**, 765–771.
43 L. N. Arnaudov, O. J. Cayre, M. a Cohen Stuart, S. D. Stoyanov, and V. N. Paunov, *Phys. Chem. Chem. Phys.*, 2010, **12**, 328–31.
44 R. A. Alvarez-Puebla and L. M. Liz-Marzan, *Chem. Soc. Rev.*, 2012, **41**, 43–51.
45 S. Yun, Y. Park, S. K. Kim, and S. Park, *Anal. Chem.*, 2007, **79**, 8584–8589.
46 W.-L. Zhai, D.-W. Li, L.-L. Qu, J. S. Fossey, and Y.-T. Long, *Nanoscale*, 2012, **4**, 137–42.
47 Y. H. Ngo, D. Li, G. P. Simon, and G. Garnier, *Langmuir*, 2012, **28**, 8782–8790.
48 L. L. He, N. J. Kim, H. Li, Z. Q. Hu and M. S. Lin, *J. Agric. Food Chem.*, 2008, **56**, 9843–9847.
49 K. R. Strehle, D. Cialla, P. Ro, T. Henkel, and M. Ko, *Anal. Chem.*, 2007, **79**, 1958–1963.
50 E. J. Liang, X. L. Ye, and W. Kiefer, *J. Phys. Chem. A*, 1997, **5639**, 7330–7335.
51 L. L. He, M. S. Lin, H. Li and N. J. Kim, *J. Raman Spectrosc.*, 2010, **41**, 739–744.
52 M. Lin, L. He, J. Awika, L. Yang, D. R. Ledoux, H. Li and a Mustapha, *J. Food Sci.*, 2008, **73**, T129–T134.
53 P. Guo, D. Sikdar, X. Huang, K. J. Si, W. Xiong, S. Gong, L. W. Yap, M. Premaratne and W. Cheng, *Nanoscale*, 2015, **7**, 2862–2868.